J. Am. Chem. Soc. **1994,** *116,* 10557−10563

Photoinduced Electron Transfer Reactions in Zeolite-Based Donor−Acceptor and Donor−Donor−Acceptor Diads and Triads

Edward H. Yonemoto,[†] Yeong Il Kim,[‡] Russell H. Schmehl,[§] Jim O. Wallin,[‡] Ben A. Shoulders,[‡] Benny R. Richardson,[⊥] James F. Haw,[⊥] and Thomas E. Mallouk[*,†]

Contribution from the Departments of Chemistry, The Pennsylvania State University, University Park, Pennsylvania 16802, Tulane University, New Orleans, Louisiana 70118, and Texas A&M University, College Station, Texas 78743, and Department of Chemistry and Biochemistry, The University of Texas at Austin, Austin, Texas 78712

Received May 16, 1994[⊗]

Abstract: Electron transfer (ET) reactions in a series of donor−acceptor (D−A) molecules (2,2′-bipyridine)$_2$Ru(4-CH$_3$-2,2′-bipyridine-4′)-(CH$_2$)$_n$-(4,4′-bipyridinium-CH$_3$)$^{4+}$ (n = 2−5, 7, 8) exchanged onto the surface of large-pore zeolites (Y, L, and mordenite) were studied in suspensions by nanosecond flash photolysis/transient diffuse reflectance techniques. From solid state CP-MAS spectra of ^{13}C-labeled compounds, it was established that the D−A molecules occupy surface sites in which the A end is occluded by the zeolite channels, while the size-excluded D end is exposed. The rate of forward ET reactions from photoexcited D to A decreases with increasing spacer length. The back ET reaction is approximately 10^5 times slower for D−A diads on the zeolite surface than in solution. Slowing of the back ET rate and a maximum in charge separation quantum yields at n = 4, 5 are attributed to lateral charge transfer diffusion on the zeolite surface to form an intermolecular charge-separated state. Addition of size- or charge-excluded electron donors (D′) to the suspension gives a D′−D−A triad, in which the initial ET reaction can be between D and A, or D′ and D, depending on energetics and the spacer length n. In both cases a long-lived charge-separated state is formed between D′ and A.

Electron transfer (ET) reactions in microheterogeneous media have been widely studied because of their potential applicability in photochemical energy conversion.[1] The spatial organization imparted to electron donors and acceptors in a solid or at a solid−liquid interface allows one to exert some control over the rates of intermolecular ET. Clever schemes for integrating various solids, such as oxide semiconductors,[2] clays,[3] zeolites,[4] sol−gel glasses,[5] and layered metal phosphonates,[6] into supramolecular electron transport systems have been described. All of these materials have unique virtues, and different effects are exploited in each to enhance the lifetime of photoinduced charge separation or to facilitate the coupling of ET events to redox catalysts or to an external electrical circuit.

Zeolites are particularly interesting organizing media for supramolecular photochemical systems, because of their structurally well-defined micropore frameworks and ion-exchange behavior. The framework charge density may be varied in order to alter the density of anchoring sites for electroactive molecules and to adjust the polarity of the microenvironment.[7] In addition,

---

[†] The Pennsylvania State University.

[‡] The University of Texas at Austin.

[§] Tulane University.

[⊥] Texas A&M University.

[⊗] Abstract published in *Advance ACS Abstracts,* October 15, 1994.

(1) (a) Grätzel, M.; Kalyanasundaram, K., Eds. *Kinetics and Catalysis in Microheterogeneous Systems*; Marcel Dekker: New York, 1991. (b) Fox, M. A.; Chanon, M., Eds.; *Photoinduced Electron Transfer*; Elsevier: Amsterdam, The Netherlands, 1988.

(2) (a) Nazeeruddin, M. K.; Kay, A.; Rodicio, I.; Humphry-Baker, R.; Müller, E.; Liska, P.; Vlachopoulos, N.; Grätzel, M. *J. Am. Chem. Soc.* **1993**, *115*, 6382 and references therein. (b) Patrick, B.; Kamat, P. V. *J. Phys. Chem.* **1992**, *96*, 1423. (c) Amadelli, R.; Argazzi, R.; Bignozzi, C. A.; Scandola, F. *J. Am. Chem. Soc.* **1990**, *112*, 7099. (d) Kim, Y. I.; Samer, S.; Huq, M. J.; Mallouk, T. E. *J. Am. Chem. Soc.* **1991**, *113*, 9561. (e) Kim, Y. I.; Atherton, S. J.; Brigham, E. S.; Mallouk, T. E. *J. Phys. Chem.* **1993**, *97*, 11802. (f) Nakato, T.; Kazuyuki, K.; Kato, C. *Chem. Mater.* **1992**, *4*, 128. (g) Nakato, T.; Kuroda, K; Kato, C. *J. Chem. Soc., Chem. Commun.* **1989**, 1114. (h) Miyata, H.; Sugahara, Y.; Kuroda, K.; Kato, C. *J. Chem. Soc., Faraday Trans. 1* **1988**, *84*, 2677.

(3) (a) White, J. R.; Bard, A. J. *J. Electroanal Chem.* **1986**, *197*, 233. (b) Villemure, G.; Detellier, C.; Szabo, A. G. *J. Am. Chem. Soc.* **1986**, *108*, 4658. (c) Ghosh, P. K.; Bard, A. J. *J. Phys. Chem.* **1984**, *88*, 5519. (d) Kovar, L.; DellaGuardia, R.; Thomas, J. K. *J. Phys. Chem.* **1984**, *88*, 3595.

(4) (a) Faulkner, L. R.; Suib, S. L.; Renschler, C. L.; Green, J. M.; Bross, P. R. In *Chemistry in Energy Production*; Wymer, R. G., Keller, O. L., Eds.; John Wiley and Sons: New York, 1982; pp 99−114. (b) Persaud, L.; Bard, A. J.; Campion, A.; Fox, M. A.; Mallouk, T. E.; Webber, S. E.; White, J. M. *J. Am. Chem. Soc.* **1987**, *109*, 7309. (c) Dutta, P. K.; Incavo, J. A. *J. Phys. Chem.* **1987**, 91, 4443. (d) Krueger, J. S.; Mayer, J. E.; Mallouk, T. E. *J. Am. Chem. Soc.* **1988**, *110*, 8232. (e) Incavo, J. A.; Dutta, P. K. *J. Phys. Chem.* **1990**, *94*, 3075. (f) Kim, Y. I.; Riley, R. L.; Huq, M. J.; Salim, S.; Le, A. N.; Mallouk, T. E. In *Synthesis/Characterization and Novel Applications of Molecular Sieve Materials*; Bedard, R. L., Ed.; Materials Research Society: Pittsburgh, PA, 1991; pp 145−156. (g) Sankaraman, S.; Yoon, K. B.; Yake, T.; Kochi, J. *J. Am. Chem. Soc.* **1991**, *113*, 1419. (h) Dutta, P. K.; Turbeville, W. *J. Phys. Chem.* **1992**, *96*, 5024. (i) Dutta, P. K.; Turbeville, W. *J. Phys. Chem.* **1992**, *96*, 9410. (j) Borja, M; Dutta, P. K. *Nature* **1993**, *362*, 43. (k) Brigham, E. S.; Kim, Y. I.; Snowden, P. T.; Mallouk, T. E. *J. Phys. Chem.* **1993**, *97*, 8650.

(5) (a) Slama-Schwok, A.; Avnir, D.; Ottolenghi, M. *J. Phys. Chem.* **1989**, *93*, 7544. (b) Slama-Schwok, A.; Avnir, D.; Ottolenghi, M. *J. Am. Chem. Soc.* **1991**, *113*, 3984. (c) Slama-Schwok, A.; Avnir, D.; Ottolenghi, M. *Nature* **1992**, *355*, 240. (d) Sassoon, R. E.; Gershuni, S.; Rabani, J. *J. Phys. Chem.* **1992**, *96*, 4692.

(6) (a) Vermuelen, L. A.; Thompson, M. E. *Chem. Mater.* **1994**, *6*, 77. (b) Vermeulen, L. A.; Snover, J. L.; Sapochak, L. S.; Thompson, M. E. *J. Am. Chem. Soc.* **1993**, *115*, 11767. (c) Vermuelen, L. A.; Thompson, M. E. *Nature* **1992**, *358*, 656. (d) Ungashe, S. B.; Wilson, W. L.; Katz, H. E.; Scheller, G. R.; Putvinski, T. M. *J. Am. Chem. Soc.* **1992**, *114*, 8717. (e) Colón, J. L.; Yang, C.; Clearfield, A.; Martin, C. R. *J. Phys. Chem.* **1990**, *94*, 874. (f) Colón, J. L.; Yang, C.; Clearfield, A.; Martin, C. R. *J. Phys. Chem* **1988**, 92, 5777.

(7) Dutta, P. K; Turbeville, W. *J. Phys. Chem.* **1991**, *95*, 4087.

(8) (a) DeWilde, W.; Peeters, G.; Lunsford, J. H. *J. Phys. Chem.* **1980**, *84*, 2306. (b) Maruszewski, K.; Strommen, D. P.; Kincaid, J. R. *J. Am. Chem. Soc.* **1993**, *115*, 8345.

0002-7863/94/1516-10557$04.50/0 © 1994 American Chemical Society

a large variety of structure types is available, and some of these contain "tailor-made" sites for encapsulation of photosensitizers.[8] Consequently, it is fairly straightforward to design zeolite-based systems in which two or three electroactive molecules are separately compartmentalized. Several of these systems have been studied by transient spectroscopic techniques and found to give long-lived charge-separated states photochemically.[4]

Size- and charge-exclusion effects facilitate self-assembly in zeolites, eliminating the formidable task of synthesizing covalently linked electron donor−acceptor (D−A) supermolecules. In general, however, it is not possible in self-assembling systems to control D−A distances precisely, the way one can with D−A triads, tetrads, and pentads that contain rigid, covalent links between subunits.[9] As a result, fine-tuning of a zeolite-based system, in order to optimize charge separation lifetimes or quantum yields, is difficult. A compromise between these two extremes is to synthesize a simple D−A diad, in which the most critical distance (the one between the photosensitizer and primary electron acceptor) is tunable, and to incorporate this diad by self-assembly into a larger system of donors and acceptors. We describe in this paper the synthesis, structural characterization, and photochemistry of simple diads and triads organized according to this principle. Solid state NMR experiments establish the location and orientation of these molecules at the zeolite−solution interface. By varying the sensitizer−acceptor distance, charge separation within the diad can be optimized. Solution-phase donors, which are excluded from the zeolite on the basis of size or charge, can then be added, and the sequence of ET steps within the triad can be followed by transient spectroscopy.

Experimental Section

Materials. Zeolites L (ideal formula $K_6Na_3Al_9Si_{27}O_{72}\cdot 21H_2O$) and Y ($Na_{56}Al_{56}Si_{134}O_{384}\cdot 250H_2O$) were purchased from Union Carbide, Linde Molecular Sieves Division. Synthetic mordenite, Valfor CBV10A ($Na_8Al_8Si_{40}O_{96}\cdot 24H_2O$), was obtained from the PQ Corp. The average diameter of the zeolite particles was found to be about 1 μm. Prior to use, in order to remove extraframework iron and other ion-exchangeable impurities, the zeolite powders were stirred in 1 M aqueous NaCl for about 8 h at 50 °C and then filtered, and this process was then repeated. The powders were then stirred in water, and then filtered and washed, and these steps were repeated until the washings were free of chloride as detected with silver nitrate. The zeolites were then allowed to dry at room temperature in air.

Deionized H_2O of resistivity 18.3 MΩ-cm was obtained from a Barnstead Nanopure system. $Gd(acac)_3\cdot 3H_2O$ (acac = acetylacetonate) was purchased from ÆSAR/Johnson Matthey. THF (HPLC grade) and acetonitrile (spectrophotometric grade) were obtained from Aldrich Chemical Co. and were used as received. $^{13}CH_3I$ was purchased from Cambridge Isotope Laboratories. $K_4W(CN)_8\cdot 2H_2O$ was prepared as described by Leipoldt et al.[10] Promethazine hexafluorophosphate was prepared by dissolving the hydrochloride (Aldrich) in water and adding excess aqueous ammonium hexafluorophosphate. The colorless crystalline product was collected by suction filtration and washed with water. All other chemicals were of reagent grade quality and were used as received from commercial sources.

Compound Synthesis. The ruthenium tris(bipyridyl)viologen diads, in which the donor and acceptor subunits are covalently linked by an aliphatic spacer (2−8 CH_2 units), were prepared as described previously.[11,12] ^{13}C-labeled diads were prepared by derivatization of 4,4′-dimethyl-2,2′-bipyridine with $^{13}CH_3I$. The labeled ligands were reacted with $RuCl_3$ to give ^{13}C-labeled Ru(4-ethyl-4′-methyl-2,2′-bipyridine)$_2$-$Cl_2\cdot 2H_2O$. Because conversion of the chloride complex to the carbonate did not in this case yield a clean microcrystalline product, the chloride was used directly in subsequent reactions. Functionalized bipyridine ligands with covalently bound viologens were labeled at the viologen end by quaternization of the 4,4′-bipyridine nitrogen atom with $^{13}CH_3I$. ^{13}C-labeled Ru(4-ethyl-4′-methyl-2,2′-bipyridine)$_2Cl_2\cdot 2H_2O$ and a slight excess of the functionalized bipyridineviologen ligand (1.5 equiv) were stirred in a 1:1 ethanol/water mixture saturated with KNO_3 for 60 h at room temperature. The products were isolated by column chromatography (silica gel), eluting with 5:4:1 CH_3CN/H_2O/saturated aqueous KNO_3, as previously described for the unlabeled compounds.[11,12]

4-Ethyl-4′-methyl-2,2′-bipyridine. 4-Ethyl-4′-methyl-2,2′-bipyridine was synthesized as described by Abruña et al., except that $^{13}CH_3I$ was used.[13] The yellow-brown oil resulting from this procedure was dissolved in chloroform and eluted with ether from a short silica column. The brown impurity remains on the column, and the product elutes as a yellow band. The ether was removed by rotary evaporation, leaving a yellow oil which upon standing becomes a waxy solid. Yield: 96%. ^1H NMR ($CDCl_3$): δ 1.1 (t, $^{13}CH_3$), 1.5 (t, $^{13}CH_3$), 2.4 (s, CH_3), 2.7 (m, CH_2); 7.1, 8.3, 8.5 (aromatic).

Ru(4-ethyl-4′-methyl-2,2′-bipyridine)$_2$Cl$_2$·2H$_2$O was synthesized according to the literature method[14] using 4-ethyl-4′-methyl-2,2′-bipyridine instead of 2,2′-bipyridine. Ru(4-ethyl-4′-methyl-2,2′-bipyridine)$_2Cl_2\cdot 2H_2O$, however, did not precipitate as microcrystals when cooled in acetone, and the product was a purplish-black powder.

[Ru(2,2′-bipyridine)$_2$(4-carboxy-4′-methyl-2,2′-bipyridine)]-(PF$_6^-$)$_2$. 4-Carboxy-4′-methyl-2,2′-bipyridine was prepared by partial oxidation of 4,4′-dimethyl-2,2′-bipyridine with $KMnO_4$ in THF.[15] The product was separated from 4,4′-dicarboxy-2,2′-bipyridine by Soxhlet extraction for 2 days with acetone. The acetone was removed by rotary evaporation to give 4-carboxy-4′-methyl-2,2′-bipyridine as a white solid. ^1H NMR ($D_2O + Na_2CO_3$): δ 2.2 (s, CH_3); 7.1 (d), 7.4 (s), 7.7 (d), 8.0 (s), 8.2 (d), 8.6 (d) (aromatic). [Ru(2,2′-bipyridine)$_2$(4-carboxy-4′-methyl-2,2′-bipyridine)](PF_6^-)$_2$ was synthesized according to a literature method[16] from Ru(2,2′-bipyridine)$_2Cl_2\cdot 2H_2O$[14] (0.10 g, 2.7×10^{-4} mol), 4-carboxy-4′-methyl-2,2′-bipyridine (0.06 g, 2.8×10^{-4} mol), and 0.08 g of $NaHCO_3$. Yield: 0.20 g, 2.18×10^{-4} mol (80%). ^1H NMR (CD_3CN): δ 2.6 (s, CH_3); 7.2−8.9 (aromatic).

[1-(2-Aminoethyl)-1′-methyl-4,4′-bipyrinediium](PF$_6^-$)$_2$. 2-Bromoethylamine hydrobromide (1.4 g, 6.8×10^{-3} mol) and [1-methyl-4,4′-bipyridinium](PF_6) (2.2 g, 7.0×10^{-3} mol) were refluxed in 150 mL of acetonitrile for 10 h, after which a yellow precipitate formed. The acetonitrile was concentrated to 40 mL, and the solution was cooled in an ice bath. The yellowish solid was vacuum filtered and washed with cold acetonitrile and then ether. The hexaflorophosphate salt of the free amine was isolated by dissolving this solid in 40 mL of water and adding a concentrated aqueous solution of NH_4PF_6, together with a few drops of concentrated ammonia. Dry nitrogen was blown over the resulting yellowish solution, and after 15 min, crystals began to form. After 1 h, the solution was cooled in an ice bath, and the crystalline product was collected by vacuum filtration and washed with 5 mL of cold water. Yield: 0.35 g, 6.7×10^{-4} mol (10%). ^1H NMR (CD_3CN): δ 3.6 (t, NCH_2), 4.4 (s, N^+CH_3), 4.7 (t, N^+CH_2-); 8.4, 8.9 (aromatic).

[1-(3-Aminopropyl)-1′-methyl-4,4′-bipyrinediium](PF$_6^-$)$_2$. This compound was prepared in the same manner as [1-(2-aminoethyl)-1′-methyl-4,4′-bipyrinediium](PF_6^-)$_2$, except that 3-bromopropylamine hydrobromide was used. Yield: 14%. ^1H NMR (CD_3CN): δ 2.2 (quintet, CH_2), 2.8 (t, NCH_2-), 4.4 (s, N^+CH_3), 4.7 (t, N^+CH_2-); 8.4, 8.9 (aromatic).

[Ru(2,2′-bipyridine)$_2$(4-(((2-(1′-methyl-4,4′-bipyridinedium-1−yl)ethyl)amino)carbonyl)-4′-methyl-2,2′-bipyridine)](PF$_6^-$)$_4$·2H$_2$O. [Ru(2,2′-bipyridine)$_2$(4-carboxy-4′-methyl-2,2′-bipyridine)](PF_6^-)$_2$ (0.20 g, 0.2 mmol), [1-(2-aminoethyl)-1′-methyl-4,4′-bipyrinediium](PF_6^-)$_2$ (0.20 g, 0.4 mmol), dicyclohexylcarbodiimide (0.08 g, 0.4 mmol), and

---

(9) Gust, D.; Moore, T. A.; Moore, A. L.; Macpherson, A. N.; Lopez, A.; DeGraziano, J. M.; Gouni, I.; Bittersmann, E.; Seely, G. R.; et al. *J. Am. Chem. Soc.* **1993**, *115*, 11141 and references therein.

(10) Leipoldt, J. G.; Bok. L. D. C.; Cilliers, P. J. *Z. Anorg. Allg. Chem.* **1974**, *407*, 350.

(11) Yonemoto, E. H.; Riley, R. L.; Kim, Y. I.; Atherton, S. J.; Schmehl, R. H.; Mallouk, T. E. *J. Am. Chem. Soc.* **1992**, *114*, 8081.

(12) Yonemoto, E. H.; Saupe, G. B.; Schmehl, R. H.; Hubig, S. M.; Riley, R. L.; Iverson, B. L.; Mallouk, T. E. *J. Am. Chem. Soc.* **1994**, *116*, 4786.

(13) Abruña, H. D.; Breikiss, A. I.; Collum, D. B. *Inorg. Chem.* **1985**, *24*, 988.

(14) Lay, P. A.; Sargeson, A. M.; Taube, H. *Inorg. Synth.* **1986**, *24*, 292.

(15) (a) Sprintschnik, G.; Sprintschnik, H. W.; Kirsch, P. P.; Whitten, D. G. *J. Am. Chem. Soc.* **1977**, *99*, 4947. (b)Elliott, C. M., personal communication.

(16) Ghosh, P. K.; Spiro, T. G. *J. Am. Chem. Soc.* **1980**, *102*, 5543.

triethylamine (35 μL, 0.25 mmol) were stirred in 40 mL of acetonitrile at room temperature for 12 h under nitrogen. The solution was filtered to remove dicyclohexylurea and then evaporated to dryness. The solid was dissolved in a minimum amount of acetonitrile and chromatographed on silica gel with a 5:4:1 mixture of acetonitrile/water/saturated KNO_3, to give three bands. The first two orange bands were fluorescent. The product eluted as a third red-orange band which was broad and nonluminescent. The solvent was removed under reduced pressure to the point where KNO_3 began to crystallize, and then acetone was added to precipate the remaining KNO_3. The solution was filtered, and the acetone was removed under reduced pressure. The solid residue was redissolved in water. The product was precipitated by adding a concentrated solution of NH_4PF_6 and then vacuum filtered, washed with water and ether, and air-dried. Yield: 80 mg, 0.057 mmol (29%). ^1H NMR (CD_3CN): δ 2.6 (s, CH_3), 4.0 (quartet, CH_2), 4.4 (s, N^+CH_3), 4.8 (t, N^+CH_2); 7.2–8.9 (aromatic). Anal. Calcd (found): C 37.51 (37.44), H 3.15 (3.12), N 8.75 (8.55).

[Ru(2,2′-bipyridine)$_2$(4-(((3-(1′-methyl-4,4′-bipyridinediium-1-yl)propyl)amino)carbonyl)-4′-methyl-2,2′-bipyridine)](PF$_6^-$)$_4$·2H$_2$O. [Ru(2,2′-bipyridine)$_2$(4-(((3-(1′-methyl-4,4′-bipyridinediium-1-yl)propyl)amino)carbonyl)-4′-methyl-2,2′-bipyridine)](PF_6^-)$_4$·2H_2O was prepared in the same manner as the C2 amide, except that the propylamineviologen derivative was used. Yield: 33%. An alternate synthetic route has been described by Meyer and co-workers.[17] ^1H NMR (CD_3CN): δ 2.3 (quintet, CH_2), 2.6 (s, CH_3), 3.5 (quartet, CH_2), 4.4 (s, N^+CH_3), 4.7 (t, N^+CH_2-); 7.2–9.0(aromatic). Anal. Calcd (found): C 37.98 (37.93), H 3.26 (3.31), N 8.66 (8.63).

Sample Preparation. The ruthenium tris(bipyridyl)viologen diads were ion-exchanged from acetonitrile stock solutions of their hexafluorophosphate salts onto the zeolite surface at a loading of 2 × 10^{-6} mol of the diad per gram of solid. Typically, 1.0 g of zeolite powder was slurried with 5 mL of acetonitrile, and then an appropriate volume of stock solution, usually about 3 mL, was added. The sample was stirred for 15 min and allowed to stand for a period of hours, after which the sample was filtered and dried in air and then stored in the dark under nitrogen. The ruthenium tris(bipyridyl)viologen complexes ion-exchange onto zeolite L and mordenite quantitatively at these loadings. In the case of zeolite Y, the exchange was not quantitative, and the actual loading was determined by spectrophotometric analysis of the combined solutions and washings. The concentration of diad was subsequently adjusted to give the same loading as with the other zeolites.

^{13}C Solid State CP-MAS NMR. Zeolite samples were compacted into a sample rotor (about 0.5 cm^3) and were spun at the magic angle in a Chemagnetics CMX-300 instrument. The observed frequency was 75.33 MHz, and the decoupler freqency was 299.56 MHz. $^1H-^{13}C$ cross-polarization (CP) was achieved with a 90° pulse of 4.2 μs width. Line broadening was set at 20 Hz, and 12 000 scans were collected overnight in each run in order to improve the signal-to-noise ratio. Chemical shifts were referenced to a hexamethylbenzene external standard. The loading of the ^{13}C-labeled D–A compounds was 1.7 × 10^{-6} mol/g zeolite. In cases where the size-excluded paramagnetic probe, $Gd(acac)_3·3H_2O$, was employed, the sample was impregnated by adding 5–7 mL of a chloroform/methanol (3:1) solution containing 3 × 10^{-5} mol of the complex per gram of zeolite to the powdered sample. The resulting suspension was then stirred and dried under vacuum at room temperature.

Transient Diffuse Reflectance Spectroscopy. Typically, 30 mg of the solid ion-exchanged samples were suspended in 1.5 mL of water or acetonitrile in a quartz cuvette for the diffuse reflectance flash photolysis experiments. The suspensions were thoroughly deoxygenated by bubbling nitrogen into the cuvette before measurements were taken. Typically, 10 measurements were averaged together for the decay traces, and three measurements were averaged at each wavelength when measurements for spectra were taken. The diffuse reflectance flash photolysis experiments were carried out at the Center for Fast Kinetics Research (CFKR), University of Texas at Austin. The experimental configuration for diffuse reflectance flash photolysis has been described previously.[2e] Fits of the experimental decay curves to the Albery dispersed kinetics model,[18] eq 1, were calculated using a finite-difference Levenberg–Marquardt routine, ZXSSQ from the International Mathematical Subroutine Library (IMSL). In this equation,

$$\frac{C(t)}{C(0)} = \frac{1}{\sqrt{\pi}} \int_{-\infty}^{\infty} \exp(-x^2) \exp[-(k_{av}t) \exp(\gamma x)]\, dx \qquad (1)$$

$C(t)$ is the signal intensity at time t, k_{av} is an average rate constant, and γ is the distribution width. These calculations were done on a VAX (11/780)/VMS computer.

Transient diffuse reflectance spectral corrections were applied to the raw data in order to correct for the different penetration depths of the excitation (532 nm) and probe beams as a function of the wavelength, λ, of the analyzing light. The empirical correction factors used were[2e]

$$\text{correction factor} = 164.0 \exp[(-9.59 \times 10^{-3})\lambda] \quad \text{for } \lambda < 650 \text{ nm}$$

$$\text{correction factor} = 0.779 - (7.30 \times 10^{-4})\lambda \quad \text{for } \lambda \geq 650 \text{ nm}$$

This correction factor was also applied in the calculation of quantum yields for formation of charge-separated states, since the transient actinometer ($Ru(bpy)_3^{2+}$ ion-exchanged onto the appropriate zeolite, assumed to form the MLCT state with unit quantum yield) and sample in general had transient absorption maxima at different wavelengths. Extinction coefficients used were ϵ_{360} = 27 300 M^{-1} cm^{-1} for the $Ru(bpy)_3^{2+}$ and D–A MLCT state transients[19] and ϵ_{400} = 42 100 M^{-1} cm^{-1} and ϵ_{600} = 13 700 M^{-1} cm^{-1} for the reduced viologen (D–A charge-separated state) transients.[20]

Results and Discussion

Structure of the D–A Diads. The photosensitizer–electron acceptor compounds used in these experiments were cations bearing two positive charges on both the donor and acceptor ends. The overall 4+ charge provides for tenacious binding of these molecules to the zeolite surface, relative to less highly charged photosensitizers such as $Ru(bpy)_3^{2+}$.[4] The connecting group between the donor and acceptor was either an aliphatic chain containing n methylene units (H*n*M) or an aliphatic amide (C*n* amide).

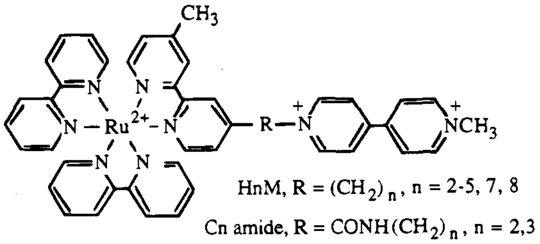

Location and Orientation of the D–A Diads at the Zeolite–Solution Interface. The maximum loading of these diads that could be achieved by ion-exchange was ca. (2–3) × 10^{-6} mol/g zeolite, consistent with approximately monolayer coverage of the zeolite external surface. The viologen end of the molecule is sufficiently small to pass through the 6.8–7.2 Å 12-ring openings of large-pore zeolites (types Y, L, and mordenite, Figure 1), but the $Ru(bpy)_3^{2+}$ end, with a diameter of 13–14 Å, is too large. This property has been exploited previously for assembly of a vectorial electron transport system, in which it was proposed[4d] that the donor and acceptor ends of structurally related molecules were respectively outside and inside the pore system. We demonstrate here that this half-in/half-out configuration is in fact the predominant binding mode for the H*n*M (*n* = 2–8) series on the surface of large-pore zeolites.

---

[17] Mecklenburg, S. L.; Meek, B. M.; Schoonover, J. R.; McCafferty, D. G.; Wall, C. G.; Erickson, B. W.; Meyer, T. J. *J. Am. Chem. Soc.* **1993**, *115*, 5479.

[18] Albery, W. J.; Bartlett, P. N.; Wilde, P.; Darwent, J. R. *J. Am. Chem. Soc.* **1985**, *107*, 1854.

[19] Kalyanasundaram, K. *Coord. Chem. Rev.* **1982**, *46*, 159.

[20] Watanabe, T.; Honda, K. *J. Phys. Chem.* **1982**, *86*, 2617.

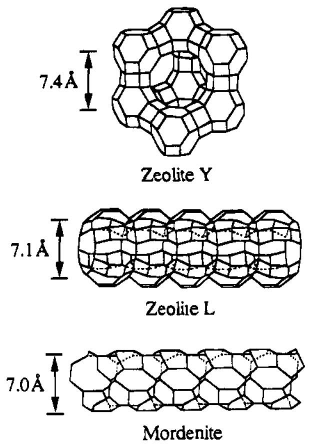

Figure 1. Framework structures of zeolites Y and L and mordenite.

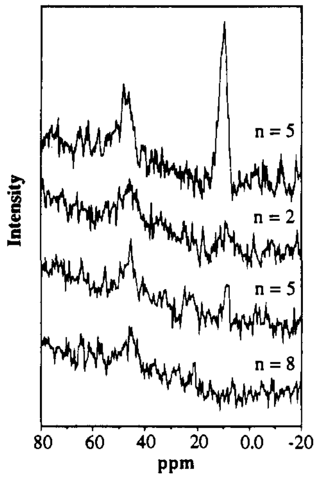

Figure 2. Solid state CP-MAS ^{13}C NMR spectra of doubly labeled H*n*M compounds on zeolite Y. The loading in all cases was 1.7 × 10^{-6} mol/g. Top: H5M on zeolite Y, with no added $Gd(acac)_3 \cdot 3H_2O$; peaks at 13 and 45 ppm are assigned to ^{13}C labels at the donor and acceptor ends of the molecule, respectively. Lower spectra: doubly labeled H2M, H5M, and H8M on zeolite Y, impregnated with 3 × 10^{-5} mol/g $Gd(acac)_3 \cdot 3H_2O$.

Figure 2 shows representative solid state CP-MAS spectra of the ^{13}C-labeled compounds exchanged onto zeolite Y. The poor signal-to-noise ratio reflects the fact that the compound is present at only monolayer coverage. The intense peak at 13 ppm may be attributed to the ^{13}C-labeled ethyl group on the two 4-ethyl-4′-methyl-2,2′-bipyridine ligands, and the peak at 45 ppm is attributed to the ^{13}C-labeled viologen methyl group. The resonances of other ^{13}C nuclei in the molecule, present at natural abundance, are too weak to be seen in the monolayer spectra. CP-MAS spectra of all the compounds studied gave similar peak positions and intensities. Impregnation of these samples with the paramagnetic probe molecule $Gd(acac)_3 \cdot 3H_2O$ caused almost complete attenuation (90–95%) of the high-field signal, whereas the low-field peak was attenuated by only 30–40%.

Complexes of Gd^{3+} are highly effective agents for inducing relaxation of nuclear spins, and they are frequently used for this purpose in solution state NMR or in magnetic resonance imaging as relaxation contrast reagents. The relaxation rate of a given spin is inversely proportional to the sixth power of its distance from the Gd^{3+} cation; thus, it should be recognized that the effect of the paramagnetic probe on ^{13}C line width for the samples considered here is highly localized. A second role of the paramagnetic agent could be to relax the protons and complicate cross-polarization. This effect could be less well localized if proton–proton spin diffusion propagated relaxation away from the Gd^{3+} site. However, protons are relatively dilute spins (chemically) in these samples, and a local influence of the paramagnetic probe seems reasonable. Since the $Gd(acac)_3 \cdot 3H_2O$ complex is size-excluded and substitution-inert, it is confined to the external surface of the zeolite. Attenuation of the high-field signal indicates that Gd ions are present in close proximity to the ^{13}C-labeled ligands at the sensitizer end of the molecule. However, the label on the viologen end, encapsulated by the zeolite framework, is predominantly inaccessible to the paramagnetic probe molecule. Interestingly, the degree of encapsulation, or "unfolding" of the diad into an extended conformation, appears to be relatively independent of the length of the spacer chain, as judged by the intensity of the low-field peak.

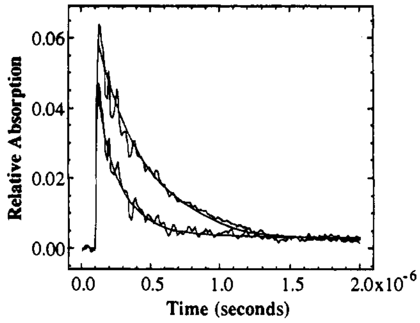

Figure 3. MLCT transient decays, monitored at 360 nm, for 2.0 × 10^{-6} mol/g $Ru(bpy)_3^{2+}$ (upper trace) and H4M (lower trace) on mordenite (aqueous suspensions). Solid lines superimposed on the experimental data are single exponential fits.

Intramolecular ET in Zeolite-Bound D–A Diads. The kinetics of light-induced forward and reverse ET reactions within the H*n*M diads in homogeneous solutions have been previously studied.[11,12] Following photoexcitation to generate the metal-to-ligand charge transfer (MLCT) state, the $Ru(bpy)_3^{2+}$ sensitizer transfers an electron to the viologen end of the molecule. The time scale of this reaction is tens of picoseconds to hundreds of nanoseconds, depending on the length of the spacer and its conformation.[12] The back ET reaction to regenerate the ground state is faster than the forward reaction by at least 1 order of magnitude for the longer spacer chains, and for the H5M–H8M compounds it is so fast that a charge-separated state cannot be observed.

For the H2M–H8M diads ion-exchanged onto the surface of zeolites Y, L, and mordenite, forward ET can be monitored by observing the decay of the MLCT excited state at 360 nm. Figure 3 shows a representative decay trace for H4M on mordenite compared to $Ru(bpy)_3^{2+}$ exchanged onto the same zeolite. The excited state decays much more rapidly in the case of the D–A molecule as a consequence of the available ET pathway. For the shortest spacer chains, MLCT lifetimes are shorter than 30 ns and could not be measured by the transient diffuse reflectance technique. For longer chains (H3M–H8M), forward ET occurs 1–2 orders of magnitude more slowly on the zeolite surface than it does in fluid solution. Two effects contribute to the retardation of the forward ET reaction. First, the molecules can explore many different conformations on the time scale of ET reactions in solution, because they contain flexible aliphatic spacers. Much of this conformational flexibility is lost by immobilization on the zeolite surface. Second, exchange of the complex onto the zeolite reduces the thermodynamic driving force for the weakly exoergic forward ET reaction.[4d,21]

In Figure 3, it can be seen that the height of the MLCT transient, extrapolated to zero time, is smaller for the D–A diad

---

[21] Li, Z.; Mallouk, T. E. *J. Phys. Chem.* **1987**, *91*, 643.

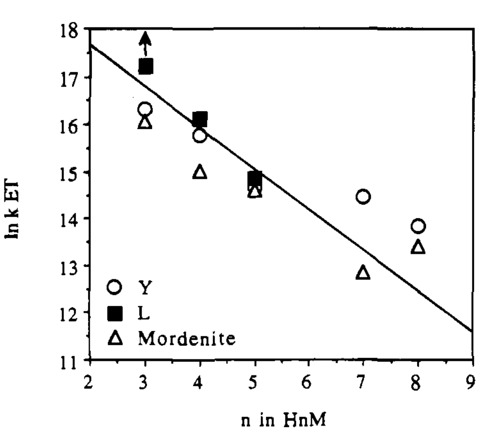

Figure 4. Plot of ln k_{ET} vs n for forward ET in HnM diads on zeolites. The slope of the solid line is 0.86.

than it is for $Ru(bpy)_3^{2+}$. The difference is largest for the shortest spacers (H3M, H4M) and smallest for the longest spacers (H7M, H8M). This difference represents a static component of MLCT quenching, which may reflect a population of diads that are folded on the surface rather than extended into the zeolite channel. For H3M and H4M, this static fraction is 25−50%, whereas for H8M it is 1−15%, depending on zeolite type.

Figure 4 shows a plot of ln k_{ET} for the forward electron transfer reaction vs the length of the spacer chain in HnM.[22] While there is some uncertainty in the ET rates, particularly for the longest spacers, where the MLCT decay is dominated by non-ET pathways, the trend toward slower rates with increasing chain length is evident. The rate constant decreases by approximately 1 natural log unit per methylene added to the spacer, and the distance dependence is apparently greater for zeolites L and mordenite and less for zeolite Y. These results parallel previous studies of forward ET within these D−A complexes in solution, in which a linear conformation was imposed on the longest spacer chains by complexation with β-cyclodextrin.[12] In the cases of zeolite L and mordenite, a linear conformation is possible for H7M and H8M. For zeolite Y, CPK models show that the conformation must be partially folded, because of the tetrahedral rather than linear interconnectivity of supercages. It is possible that these conformational restrictions are responsible for different distance dependences of ET rate in the three zeolites.

Charge Separation and Back ET in D−A Diads. Although back ET reactions are in general very fast in solution for the HnM series, these diads give long-lived charge-separated states on the zeolite surface. Figure 5 shows a typical set of UV−visible diffuse reflectance spectra following 532 nm laser excitation of H5M on mordenite. Positive transients at 390 and 600 nm can be attributed to formation of the viologen radical cation ($MV^{\bullet+}$), and the negative transient at 450 nm reflects the formation of $Ru(bpy)_3^{3+}$, i.e., bleaching of the ground state $Ru(bpy)_3^{2+}$ absorbance. These spectral features decay together, for all of the HnM and Cn amide D−A compounds, on a time scale of tens to hundreds of microseconds. By way of comparison, the time scale for back ET in H5M is less than 10 ns in fluid solution.

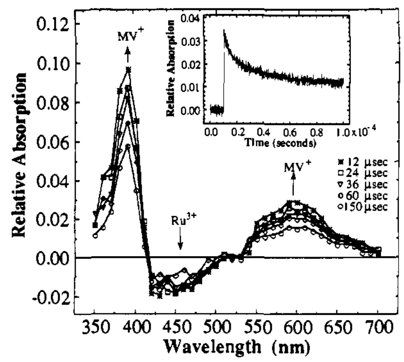

Figure 5. Transient UV−visible diffuse reflectance spectra for H5M on mordenite, recorded 12−150 μs after 532 nm laser excitation. Inset shows the rapid rise and slow decay of the $MV^{\bullet+}$ signal at 400 nm. Solid line through the decay represents a best fit to the dispersed kinetics model with $k_{av} = 2.56 \times 10^4\ s^{-1}$.

Table 1. Charge Separation Quantum Yields and Back ET Rates, Monitored at 400 nm, for HnM on Zeolites

zeolite/HnM	quantum yield	k_{av}	γ
Y/2	0.007	2.39×10^5	7.8
3	0.023	1.65×10^5	5.1
4	0.040	1.13×10^5	3.8
5	0.049	5.43×10^4	4.0
7	0.018	3.84×10^4	3.8
8	0.014	2.44×10^4	2.3
L/2	0.010	4.80×10^5	13.5
3	0.017	1.57×10^5	8.2
4	0.047	4.47×10^4	7.8
5	0.072	2.38×10^4	3.9
7	0.026	3.58×10^3	5.2
8	0.016	6.52×10^3	0.0
mordenite/2	0.024	2.43×10^5	2.6
3	0.040	9.20×10^4	3.1
4	0.049	7.75×10^4	3.0
5	0.060	2.56×10^4	3.9
7	0.023	2.15×10^4	2.5
8	0.020	1.19×10^4	5.8

While the forward ET reaction follows simple first-order kinetics, back ET in the D−A diads on the zeolite surface is kinetically complex. The inset in Figure 5 shows the decay of the $MV^{\bullet+}$ transient signal at 400 nm for H5M on mordenite. There is a rapid initial decay of the charge-separated state, followed by a longer-lived transient that decays over a time scale of hundreds of microseconds. Because simple kinetic models failed to fit these data, the dispersed kinetics model developed by Albery and co-workers[18] was used. This model, which is appropriate for kinetic processes in many heterogeneous media, assumes a Gaussian distribution of activation energies about some average value. The virtue of the model in the present case is that it represents the data with relatively few parameters: a preexponential factor, from which the quantum yield for charge separation can be calculated; an average decay rate, k_{av}; and a parameter, γ, related to the width of the Gaussian distribution. For low values of γ, the fit approaches a simple first-order decay with rate constant k_{av}. Table 1 shows values of the quantum yields, k_{av}, and γ values calculated for HnM on different zeolites.

The trend in quantum yields for formation of the long-lived charge-separated states in HnM diads is plotted in Figure 6. The maximum quantum yield occurs at $n = 5$.[23] For longer spacers, the yield drops off because the forward ET reaction is less competitive with other modes of MLCT decay. For shorter spacers, however, the low quantum yields are at first surprising, in light of the efficiency of the forward ET reaction and the apparent slowness of back ET. A reasonable model to explain these trends involves lateral charge transfer diffusion, between $Ru(bpy)_3^{3+}$ and $Ru(bpy)_3^{2+}$ and/or between $MV^{\bullet+}$ and MV^{2+}, on the zeolite surface. That is, the very long lifetime of the observed $Ru(bpy)_3^{3+}$−$MV^{\bullet+}$ state—a factor of 10^5 longer than

---

[22] k_{ET} was calculated from the rate constant of the HnM MLCT decay at 360 nm and that of $Ru(bpy)_3^{2+}$ (k_0) on the same zeolite: $k_{ET} = k_{MLCT} - k_0$.

[23] Similar trends were found for the Cn amide series. Charge separation quantum yields were 5−7% for $n = 2, 3$ on the three zeolites studied.

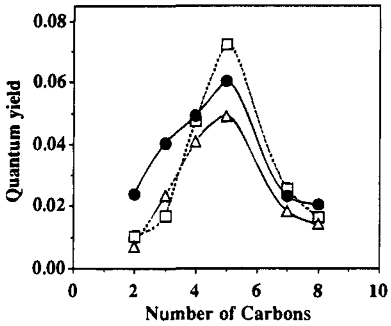

Figure 6. Transient quantum yields for charge-separated state formation in H*n*M diads on zeolites in aqueous suspensions. Quantum yields were calculated by comparing the height of $MV^{\bullet+}$ transient at 400 nm to the MLCT transient of $Ru(bpy)_3{}^{2+}$ (at 360 nm) on the same zeolite.

in solution for H5M, for example—reflects inter- rather than intramolecular charge separation. Intramolecular back ET might be expected to occur on a time scale of nanoseconds in these compounds, and to slow down with increasing chain length. If, however, these molecules are juxtaposed with their neighbors at favorable distances, the slower of these back ET reactions will be intercepted by lateral charge transfer on the surface. The maximum in charge separation quantum yield at $n = 5$ represents a combination of slow intramolecular back ET, kinetically competitive electron exchange with neighboring D−A molecules, and efficient ET quenching of the MLCT excited state.

The fact that the charge separation quantum yield is low (1−5%) for all chain lengths indicates that the rate of back electron transfer within the D−A diads is in all cases faster than the lateral charge transfer rate. The latter can be estimated from the intermolecular distance of $Ru(bpy)_3{}^{2+}$ units on the zeolite surface and the bimolecular self-exchange rate of the $Ru(bpy)_3{}^{3+/2+}$ couple, k_{ex}. Following the treatment of Majda and co-workers,[24] the rate of the self-exchange reaction in two dimensions is given by eq 2, where ${}^{2D}k_{ex}$ is the two-dimensional

$$\text{rate} = {}^{2D}k_{ex}\Gamma = k_{ex}\Gamma/2r \qquad (2)$$

electron transfer rate constant, expressed in units of $cm^2\ mol^{-1}\ s^{-1}$, Γ is the coverage of electroactive units on the surface, and r is the intermolecular separation. Using $\Gamma = 2 \times 10^{-10}$ mol cm^{-2}, $r = 10^{-7}$ cm, and the literature value[25] of k_{ex} (9×10^9 $cm^3\ mol^{-1}\ s^{-1}$), we estimate a surface self-exchange rate on the order of $10^7\ s^{-1}$. This rate is approximately 10 times slower than that of the back ET reaction in the H5M diad, consistent with the low quantum yields (5−7%) observed for charge separation in that case. In the case of the shorter spacers, the back ET reaction is very fast relative to lateral charge transfer, and the observed quantum yield is lower. For the longer chains, lateral charge transfer is more competitive with back ET, but the fraction of excited states quenched by the forward ET reaction is low, again resulting in lower charge separation quantum yields.

Zeolite-Based Donor−Donor−Acceptor Triads. Having characterized the zeolite-based D−A diads with respect to forward and back ET reactions, it is possible to add another element of complexity by including secondary electron donors and acceptors. In a previous paper, we showed that the addition of cationic intrazeolite acceptors extended the lifetime of charge separation.[4d] Here, we show that solution-phase electron donors (D′) can be coupled to the D−A diads in two ways. These two modes of operation are illustrated in Scheme 1. If forward ET within the D−A diad is fast relative to ET between D′ and D* (the excited state of D), then the sequence of electron transfer events depicted in case 1 is followed. The efficiency of charge separation is at best the same as in the D−A diad, but the charge-separated state is $D'^{+}-D-A^{-}$ rather than $D^{+}-A^{-}$. On the other hand, if forward ET within the diad is slow, then D′ quenches the diad excited state via electron transfer (case 2). The final charge-separated state is the same, but the efficiency of charge separation is now determined by the rate of back ET within the $D'^{+}-D^{-}$ geminate pair, relative to forward ET between D^{-} and A.

Figure 7 illustrates a case 1 triad system, in which the electron donor is the promethazine cation (PMZ^{+}). This cation, which is size-excluded from the zeolite, is a sufficiently good reducing agent ($E_o' = +0.94$ V vs SCE in CH_3CN) to donate an electron to Ru^{3+} ($E_o' = +1.23$ V), but not to Ru^{*2+} ($E_o' = +0.77$ V).[26] The transient spectra in Figure 7 clearly show that the final charge-separated state is $PMZ^{\bullet 2+}-Ru(bpy)_3{}^{2+}-MV^{\bullet+}$ in the presence of PMZ^{+}. With surface-bound D−A diads such as H*n*M (n = 4,5) and C*n* amide (n = 2,3), forward ET is fast, and the promethazine cation cannot quench the $Ru(bpy)_3{}^{*2+}$ excited state. The transient decays in Figure 8 show that the rise of the $MV^{\bullet+}$, viewed on the microsecond time scale, is essentially instantaneous, consistent with rapid forward ET in the D−A diad. The rise of the $PMZ^{\bullet 2+}$ signal at 510 and the

Scheme 1. Two Kinetic Pathways for Electron Transfer in D′−D−A Triads

Case 1: initial electron transfer is D* ⟶ A

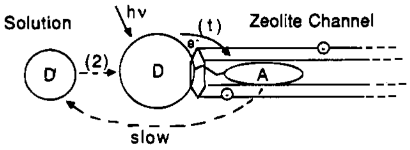

Case 2: initial electron transfer is D′ ⟶ D*

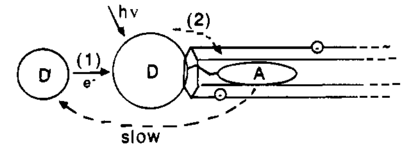

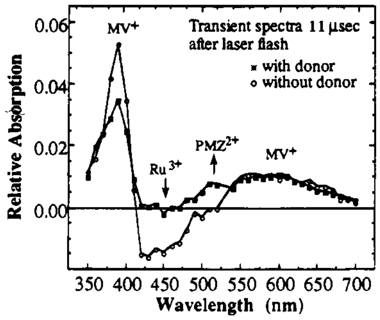

Figure 7. Transient UV−visible spectra for the PMZ^{+}−H5M triad on mordenite (acetonitrile suspension) following 532 nm excitation. In the absence of PMZ^{+}, absorbance maxima at 390 and 600 nm and bleaching at 450 nm indicate formation of a $Ru^{3+}-MV^{\bullet+}$ charge-separated state. In the presence of 5 mM PMZ^{+}, bleaching recovery at 450 nm and a new transient absorbance at 510 nm show that the $Ru^{3+} + PMZ^{+} \rightarrow Ru^{2+} + PMZ^{2+}$ ET reaction is complete within 11.8 µs.

---

[24] (a) Charych, D. H.; Landau, E. M.; Majda, M. *J. Am. Chem. Soc.* **1991**, *113*, 3340. (b) Majda, M. In *Kinetics and Catalysis in Microheterogeneous Systems;* Grätzel, M., Kalyanasundaram, K., Eds.; Surfactant Science Series 38; Marcel Dekker: New York, 1991; pp 227−272.

[25] Chan, M. S.; Wahl, A. C. *J. Phys. Chem.* **1978**, *82*, 2542.

[26] Ground and excited state formal potentials for the electron donor moiety were determined by cyclic voltammetry of H*n*M and of the model complex Ru(4,4′-dimethyl-2,2′-bipyridine)(2,2′-bipyridine)$_2{}^{2+}$ in acetonitrile/0.1 M $TBA^{+}BF_4{}^{-}$. The excess free energy of the MLCT excited state is 2.08 eV (ref 12).

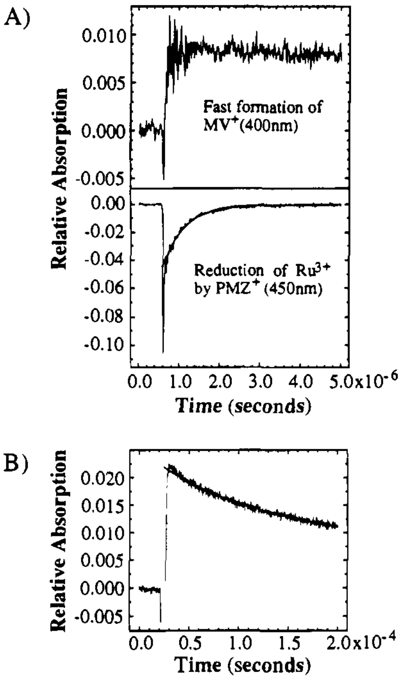

Figure 8. (A) Transient decays of H5M/mordenite with 5 mM PMZ$^+$ (acetonitrile suspension). Upper trace shows that D−A ET to form MV$^{\bullet+}$ is very fast on a 5 μs time scale; lower trace shows bleaching recovery concomitant with ET from PMZ$^+$ to Ru^{3+}. (B) Decay of the PMZ$^{\bullet 2+}$ − MV$^{\bullet+}$ charge-separated state, monitored at 600 nm. Solid line is a second-order fit to the data.

recovery of the absorbance Ru(bpy)$_3^{2+}$ at 450 nm occur concurrently on a time scale of a few microseconds, because the second electron transfer step is from PMZ$^+$ to Ru(bpy)$_3^{3+}$. The charge-separated state then collapses back to the ground state via second-order kinetics, on a time scale of several hundred microseconds. The fact that the decay of the charge-separated state follows second-order kinetics implies that the oxidized donor, PMZ$^{\bullet 2+}$, escapes from the zeolite surface before back electron transfer occurs. We note that the time scales of the D$^+$−A$^-$ (Figure 5) and D$'^+$−D−A$^-$ (Figure 8) decays are comparable, but the kinetics are quite different: complex heterogeneous kinetics in the case of the (intermolecular) D$^+$−A$^-$ charge-separated state and simple second-order kinetics for D$'^+$−D−A$^-$.

Figure 9 shows the formation and decay of the charge-separated state in a case 2 triad, where aqueous W(CN)$_8^{4-}$ acts as an electron donor quencher for photoexcited H8M. High concentrations of W(CN)$_8^{4-}$ were required for efficient quenching, presumably because of the negative surface charge of the zeolite,[27] and under these conditions it was not possible to collect data in the blue region of the spectrum. With no electron donor in solution, the D$^+$−A$^-$ charge-separated state is formed in ca. 2% quantum yield, since forward electron transfer across the 8-carbon spacer does not compete effectively with other modes of MLCT decay. Addition of 15, 45, and 75 mM W(CN)$_8^{4-}$ quenches 64, 91, and 96%, respectively, of the MLCT emission, consistent with efficient D$'$−D* electron transfer. Interestingly, the second ET reaction, which generates the reduced acceptor, MV$^{\bullet+}$, is complete on a submicrosecond time scale. Since this ET proceeds from Ru(bpy)$_3^+$, rather than Ru(bpy)$_3^{*2+}$, there is ca. 400 mV additional driving force for formation of the D$'^+$−D−A$^-$ charge separated state, and the second ET reaction is therefore very fast even across the longest spacer. Consistent with the series of ET steps in case 2, the quantum yield for charge separation is 10%, higher than in any of the simple D−A diads. In this case, the quantum yield is most probably limited by cage escape efficiency of W(CN)$_8^{3-}$/Ru(bpy)$_3^+$ geminate ion pairs.[27]

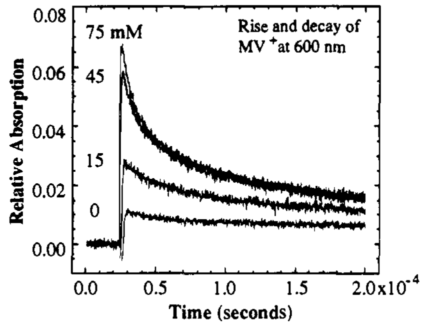

Figure 9. Transient decays monitored at 600 nm for H8M/mordenite in aqueous K$_4$W(CN)$_8$·2H$_2$O solutions at 0, 15, 45, and 75 mM concentration. At low concentrations, the first few data points were eliminated to remove a large negative transient arising from MLCT emission.

Conclusions

Ru(bpy)$_3^{2+}$−viologen donor−acceptor diads bind to the surface of large-pore zeolites in a half-in/half-out conformation. The rates of intramolecular forward ET within these diads reflect the extended conformation of their aliphatic spacer chains, and long-lived charge-separated states are formed by competition of intermolecular electron exchange with intramolecular back ET. By adding size- or charge-excluded electron donors to suspensions of these D−A systems, it is possible to extend the lifetime and/or quantum yield for charge separation by formation of a D$'^+$−D−A$^-$ charge-separated state. The length of the spacer in the D−A diad determines the efficiency of charge separation and the sequence of electron transfer steps within the triad. One may easily envision more complex systems containing, for example, secondary electron acceptors within the zeolite pore network or reservoirs of electron-donating groups on soluble polyelectrolytes or separate solid particles, which could further improve the yields and/or lifetimes of photochemical charge separation in these systems. These possibilities will be explored in future experiments.

Acknowledgment. We thank Professor C. M. Elliott for helpful advice on ligand synthesis. This work was supported by the Division of Chemical Sciences, Office of Basic Energy Sciences, Department of Energy, under contract DE-FG02-93ER14374, and by the Welch Foundation. Work at Texas A&M was supported by the National Science Foundation (CHE-9221406). Flash photolysis experiments were carried out at the Center for Fast Kinetics Research (CFKR), University of Texas at Austin. The CFKR is supported jointly by the Biomedical Research Technology Program of the Division of Research Resources of NIH (RR00886) and by the University of Texas at Austin. T.E.M. thanks the Camille and Henry Dreyfus Foundation for support in the form of a Teacher-Scholar Award.

---

(27) In fluid aqueous solution, ion pairing between W(CN)$_8^{4-}$ and Ru(bpy)$_3^{2+}$ occurs, and ET quenching of the MLCT state is efficient, even at very low concentration of W(CN)$_8^{4-}$: Mallouk, T. E.; Krueger, J. S.; Mayer, J. E.; Dymond, C. M. *Inorg. Chem.* **1989**, *28*, 3507.